



INVESTIGATING NOVEL MIXED HALIDE PEROVSKITE MATERIAL $\text{CH}_3\text{NH}_3\text{Pb}(\text{I}_{1-x}\text{Cl}_x)_3$ TO OBTAIN OPTIMIZED PCE OF ABOVE 30% IN PEROVSKITE SOLAR CELL

Ms. Nishi Bala, Assistant Professor, Dept. Of Electrical and Electronics Engineering, Bakhtiyarpur College of Engineering, Champapur, Dedaaur, Bakhtiyarpur, Bihar, India.

Mr. Abhishek Raj, Research Scholar, Dept. of Mechanical Engineering, National Institute of Technology, Jamshedpur, Adityapur, Jamshedpur, Jharkhand, India.

Abstract

Because of its significant increase in efficiency over last decade, the perovskite solar cell (PSC) has become most sought area of research in the photovoltaic technology. In this paper, Effect of variation of defect density in combination with different width of perovskite absorption layer has been investigated to obtain optimum solar cell parameters like FF, Voc, Isc and PCE. Comprehensive simulation approach has been utilized with SCAPS 1D software. Major objective of present work is to analyze different defect density and thickness value of perovskite absorption layer for achieving the optimized parameter like PCE. The proposed device structure utilized TiO_2 as an electron transport layer (ETL), Spiro-OMeTAD as a hole transport layer (HTL), mixed halide $\text{CH}_3\text{NH}_3\text{Pb}(\text{I}_{1-x}\text{Cl}_x)_3$ as perovskite absorption layer (PAL), Fluorine doped tin oxide (FTO) as top electrode and Au as anode contact. The simulation results shows that at the thickness of 900 nm and defect density of $1 \times 10^{12} \text{ cm}^{-3}$ of PAL, the optimized parameters obtained, namely PCE 30.93%, Voc 1.45 V, Jsc 25.48 mA/cm² and fill factor (FF) 83.92%. The optimization of thickness in combination with reduced defect density provided a superior power conversion efficiency (PCE) above 30%, much greater than the earlier reported value for the PSCs. Also, effect of variation of interface defect density between ETL/PAL and between PAL/HTL on the PCE is also investigated and simulated with the help of SCAPS-1D.

Keywords: ETL-Electron transport layer, PSC- Perovskite Solar Cell, PAL – Perovskite Absorption Layer, PCE – Power Conversion Efficiency, HTL-Hole transport layer

Introduction

The perovskite materials having compound structure ABX_3 which is a combination of organic and inorganic material was instrumental in transforming the area of organic-inorganic hybrid solar cells. The perovskite material having general structure ABX_3 [1], where A is methyl ammonium ion (MA^+) [2], B is an inorganic material mainly Pb or Sn [3], and X is halide or halide compounds [4-5]. Due to its superior optoelectronic properties [6] like high solar photon absorption in comparison to silicon solar cell [7-9], higher PCE, the PSC evolved as the best option in recent decades.

PSC has become the most sought photovoltaic technology due to perovskite's unique properties such as direct and tunable bandgap as the solar cell required direct band gap for the absorbance of photon and tunable band gap provide liberty for absorbance of range of light spectrum of different wavelength, low carrier binding energy, which allow easy generation of charge carrier even on the absorbance of low energy photon, high conductivity, long electron-hole diffusion length, which provide longer life time to carriers in turn higher current density and PCE, high carrier mobility, high absorption coefficient [10]–[11], less cost and its abundant availability on earth [12]–[13].

For utilizing aforesaid benefits, Kojima et al proposed first PSC obtained efficiency of 3.8 % [14]. The perovskite solar cell is made up of two carrier transport layers (ETL and HTL) and the perovskite absorption layer (PAL) [15]. The PAL is a light harvesting layer and its principal function is to absorb photons and generate charge carrier pairs. Function of Both carrier transport layers (ETL



and HTL) is to extract and deliver the generated electrons and holes to electrodes to contribute current [16]–[17].

Despite the numerous benefits of perovskite absorption layers, the presence of defects in PAL, introduced mainly during fabrication process reduces PSC parameter by causing hysteresis to charge carrier movement [18], recombination with charge carriers [19], carrier movement obstruction [20], scattering to Charge carriers i.e electrons and holes [21], and ion transfer [22]. Defects in perovskite absorption are type of point defects like anti-site replacements atomic vacancies [23]–[24]etc.

Taking defect energy level as parameter two type of defect is defined one is shallow defect density and another is Deep defect level. When defect energy level lie near to Valance or Conduction Band it is known as Shallow Defect and When Defect energy level lie between Conduction band and Valance Band it known as Deep defect position.

The current study aims to evaluate the effect of factors namely width and defect density of perovskite absorption layer on the performance of PSC structure FTO/TiO₂/CH₃NH₃Pb(I_{1-x}Cl_x)₃/Spiro-OMeTAD/Au, it is investigated and simulated using SCAPS-1D software. Standard deep energy defect level of 0.6 eV is considered for the current study. We have utilized TiO₂ as ETL due of its suitable band alignment and stability [25]–[26]. Mixed halide perovskite is considered as an absorber layer. In many studies and from experimental result it is found that structure MAPbX₃ (X is Cl, Br, I) provide least stability and high conversion efficiency when X is I and better stability but less efficiency when X is Cl. [27]–[28]. Therefore, mixed halide has been considered by substitution of I with Cl, which provides enhanced stability and diffusion length, accordingly, CH₃NH₃Pb(I_{1-x}Cl_x)₃ is considered as light harvesting layer for better performance [29]–[30]. As HTL, Spiro-OMeTAD is taken because ionization potential of Spiro-OMeTAD matches well with the light harvesting layer and best glass-forming properties of Spiro-OMeTAD provides good contact at their interfaces [31]. For the suggested PSC structure, basic characteristics such as V_{OC}, J_{SC}, PCE and FF were examined. The device modelling and illustration of result of different parameter requires software simulation and numerical modelling. The Solar Cell Capacitance Simulator (SCAPS) application used for this purpose [32].

This paper contains five sections. In Section 1 introduction of PSC devices its advantage and limitations, reason to choose proposed device structure and parameters that are having tremendous effect on PCE has been discussed. In the section 2 proposed device structure is introduced, its schematic diagram, energy band diagram and the carrier transport mechanism inside device has been explained. Section 3 discuss about mathematical modelling of SCAPS-1D software, equations involved in execution of simulations. In the section 4, various result of solar cell parameter that obtained by varying defect densities, width of PAL, Defect energy levels and Interface defect densities has been discussed. Optimum result of PCE that obtained on a specific design parameter has been discussed and its comparison with previous works has been done. In the section 5, Conclusions have been provided and future works recommended for further enhancement of PCE and other solar cell parameter.

Proposed Device Architecture

An organic-inorganic PSC having a configuration of FTO/TiO₂/CH₃NH₃Pb(I_{1-x}Cl_x)₃/ Spiro-OMeTAD/Au. The Proposed PSC device as shown in Fig. 1(a) is constructed using FTO, which works as a top electrode of 400 nm thickness. CH₃NH₃Pb(I_{1-x}Cl_x)₃ as PAL of thickness 900 nm, TiO₂ as an ETL of width 40 nm, Spiro-OMeTAD as a HTL of width 250 nm. Au works as the anode. Fig. 1(b) represent the working mechanism in the device, the PAL captures solar spectrum photons whose energy is more than its bandgap of 1.55 eV and generate electron and hole pairs in the conduction and valance band of the PSC respectively. Generated Holes and Electrons move towards HTL and ETL respectively.

Figure 1(a) shows Schematic of PSC device structure and Figure 1(b) demonstrate energy band diagram and the carrier transport mechanism in proposed structure. Table 1 mention use simulation parameters and material properties in this paper of $\text{CH}_3\text{NH}_3\text{Pb}(\text{I}_{1-x}\text{Cl}_x)_3$ based PSC device.

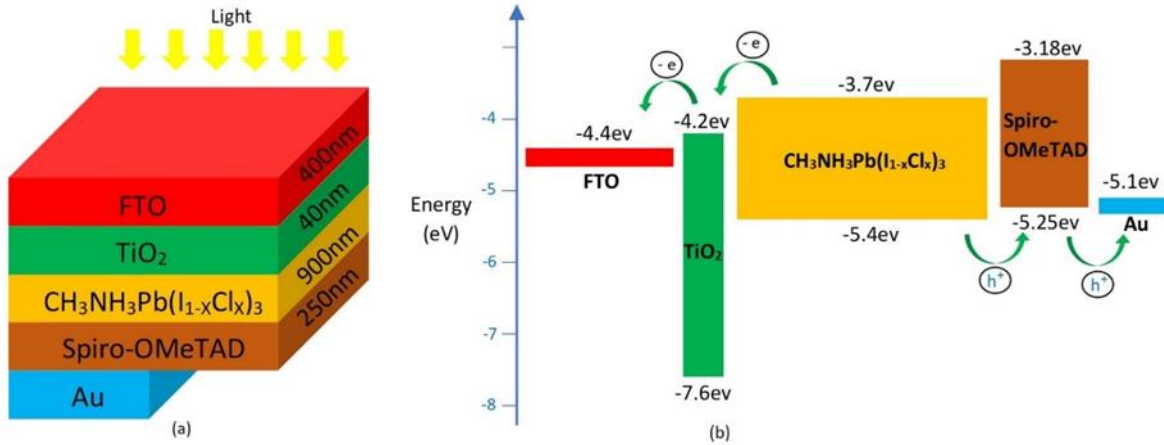


Figure 1 (a) Schematic diagram of proposed PSC device (b) Energy band diagram and the carrier transport mechanism in $\text{CH}_3\text{NH}_3\text{Pb}(\text{I}_{1-x}\text{Cl}_x)_3$ based PSC device

Fig. 1(b) shows band diagram with respect to vacuum level. Energy bands i.e. conduction band and valence band of sandwiched layers are compatible such that it allows smooth carrier transport. Electron and hole pairs are generated in perovskite absorption layer $\text{CH}_3\text{NH}_3\text{Pb}(\text{I}_{1-x}\text{Cl}_x)_3$. Electron moves in conduction band of PAL of energy level -3.7 eV to ETL energy level -4.2 eV and further collected at FTO at energy level -4.4 eV . In this way electron moves from higher energy level to comparatively lower energy level to contribute current. Hole moves in valence band of PAL of energy level -5.4 eV to HTL energy level at -5.22 eV and further collected at electrode Au at energy level -5.1 eV . Here hole moves in valence band lower energy level to comparatively higher energy level to contribute current.

Table 1 The properties of materials and simulation parameters in $\text{CH}_3\text{NH}_3\text{Pb}(\text{I}_{1-x}\text{Cl}_x)_3$ based PSC device

Parameters	Spiro-OMeTAD	$\text{CH}_3\text{NH}_3\text{Pb}(\text{I}_{1-x}\text{Cl}_x)_3$	TiO_2	FTO
Thickness (nm)	250	200-900	40	400
$E_g(\text{eV})$	3.17[34]	1.55[35]	3.2[33]	3.5[33]
Electron Affinity (eV)	2.45[34]	3.93	3.9	4[33]
Relative permittivity	3[34]	6.5[36]	9[33]	9[33]
Conduction band effective density of states $N_c(\text{cm}^{-3})$	2.2×10^{18} [34]	2.2×10^{17}	1×10^{21}	2.02×10^{18}
Valence band effective density of states $N_v(\text{cm}^{-3})$	1.9×10^{19} [34]	1.8×10^{19} [35]	2×10^{20}	1.8×10^{19} [33]
Thermal velocity of electron (cm/s)	1×10^7	1×10^7	1×10^7	1×10^7 [33]
Thermal velocity of hole (cm/s)	1×10^7	1×10^7	1×10^7	1×10^7
Mobility of electron $\mu_e(\text{cm}^2/\text{Vs})$	2×10^{-4} [34]	0.2	20	20
Mobility of hole $\mu_h(\text{cm}^2/\text{Vs})$	2×10^{-4}	0.2	10	10
Donor density $N_D(\text{cm}^{-2})$	0	0	2×10^{19}	2×10^{19}
Acceptor density $N_A(\text{cm}^{-2})$	1×10^{18}	0	0	0
$N_t(\text{cm}^{-3})$	1×10^{14}	1×10^{12} to 1×10^{16}	1×10^{15}	1×10^{15}

Mathematical Modeling

The SCAPS-1D (Solar Cell Capacitance Simulator) developed by Burgelman primarily used numerical modelling based on four set of electronic device equations, namely Poisson's equation, Continuity equations and current density equations.

Poisson's equation

$$-\frac{d^2\phi(x)}{dx^2} = \frac{dE}{dx} = \frac{\rho}{\epsilon} = \frac{q(p-n+N_D^+-N_A^- \pm N_{def})}{\epsilon_0\epsilon_r}$$

Where ϕ is electric potential, E is strength of electric field, ρ is charge density ϵ is permittivity, q is fundamental unit of charge, n and p are the concentration of electron and hole respectively. N_D^+ and N_A^- are concentration of donor and acceptor ions. N_{def} is concentration of defect density of donor and acceptor.

Continuity Equation

$$\frac{1}{q} \left(\frac{dJ_e}{dx} \right) = G - R$$

$$\frac{1}{q} \left(\frac{dJ_n}{dx} \right) = G - R$$

$\frac{dJ_e}{dx}$ is variation of electron current density with respect to position,

$\frac{dJ_n}{dx}$ is variation of hole current density with respect to position,

G is generation rate and R is recombination rate

Current Density Equation

$$J_e = q \left(n\mu_e E + D_e \frac{dn}{dx} \right)$$

$$J_n = q \left(n\mu_n - D_n \frac{dp}{dx} \right)$$

Where, J_e , J_n are electron and hole current density respectively. μ_e , μ_n are electron and hole mobility respectively. D_e , D_n are diffusion current constant

Results and discussions

The effect of variation of thickness and defect density of the PAL, i.e. $CH_3NH_3Pb(I_{1-x}Cl_x)_3$ on the PSC device has been investigated to obtain specific PSC device which provide maximum PCE. Further, impact of interface defect density of ETL/ Perovskite and HTL/ Perovskite layers on the PCE has been obtained and discussed. Standard deep energy defect level of 0.6 eV is considered. Effect of variation of defect density on the diffusion length and lifetime of carrier has also been obtained. Contour of V_{OC} , J_{SC} , FF and PCE as a joint function of defect density and PAL thickness is drawn and optimized result has been discussed.

Effect of PAL thickness variations on PSC parameters

The simulation of $CH_3NH_3Pb(I_{1-x}Cl_x)_3$ based device is established by utilizing the parameters listed in Table 2. Effect of variation of PAL thickness at the defect density of $1 \times 10^{12} \text{ cm}^{-3}$ is investigated. Variation of V_{OC} , J_{SC} , FF and PCE with respect to change of thickness from 200 nm to 900 nm is studied. It is well observed that J_{SC} continuously increased with increase of PAL thickness, provides a maximum value 25.481 mA/cm² which obtained at the PAL width of 900 nm. This may be explained as increase in PAL thickness allow absorption of more solar photon, results into increased charge carrier pairs and consequently higher current density. It is observed that J_{SC} move towards saturation with further increase in width, it happened mainly due to increased rate of recombination. V_{OC} continuously decreased with the increasing PAL thickness, at 900 nm we obtained V_{OC} of 1.446V. FF is also reduce with increase of width from 200 nm to 900 nm. The PCE is increased continuously with increase of PAL width from 200 nm to 900 nm, mainly due to

increased current density. Maximum PCE of 30.93% is obtained at 900 nm. Further increase of width caused little improvement in the PCE.

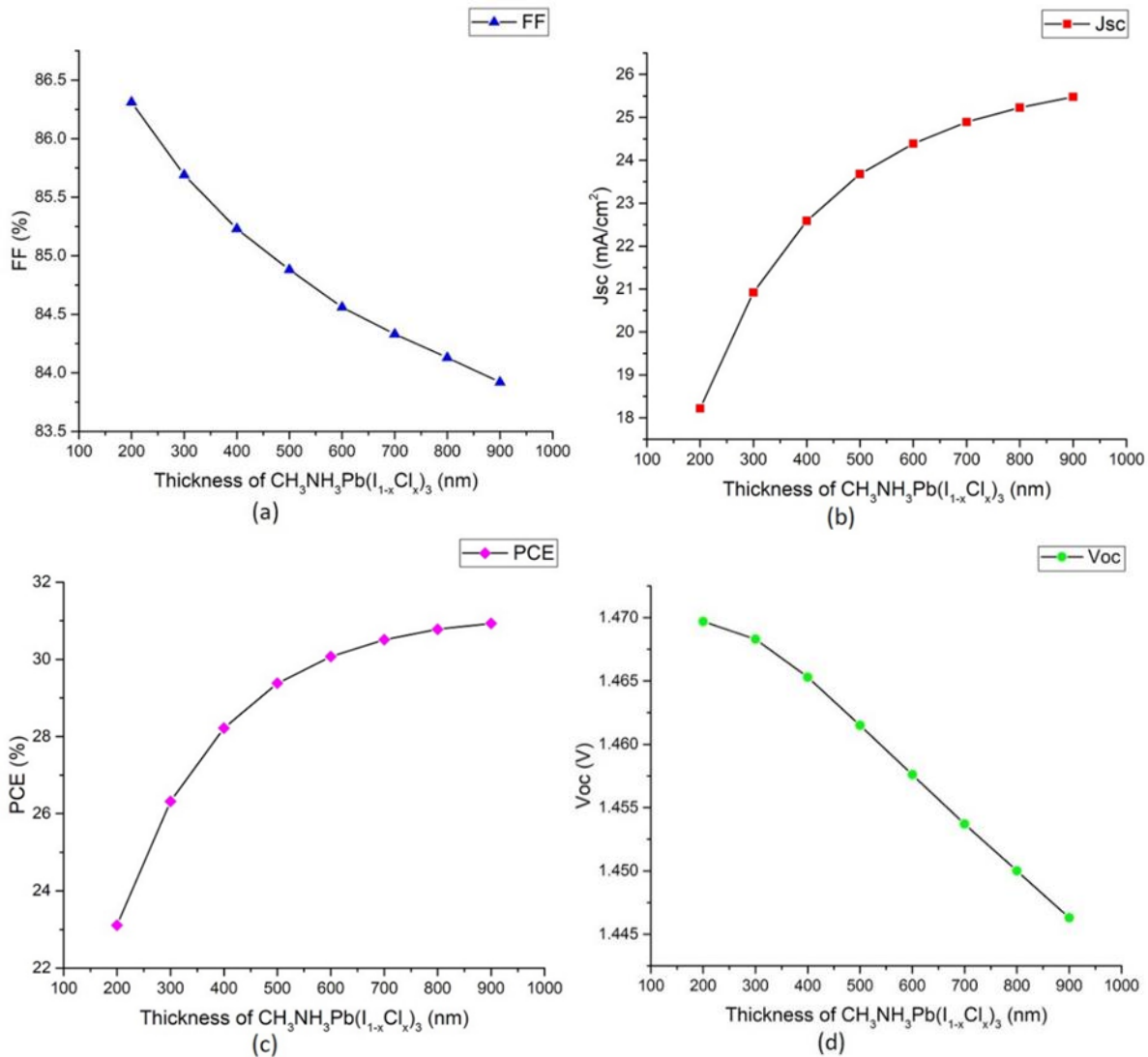


Figure 2. Showing the variation of Solar cell parameters with respect to thickness of PAL.(a) FF with respect to PAL width.(b) J_{sc} with respect to PAL width (c)Variation of PCE with respect to PAL width.(d) V_{oc} with respect to PAL width.

Impact of variations of PAL defect density on PSC parameters

Defect density of PAL, $CH_3NH_3Pb(I_{1-x}Cl_x)_3$ is varied at the obtained optimum thickness of 900 nm of PAL. Defect density of PAL varied from $1 \times 10^{12} \text{ cm}^{-3}$ to $1 \times 10^{16} \text{ cm}^{-3}$ and its effect on PSC Parameters of V_{oc} , J_{sc} , FF and the PCE is investigated. It is observed that all parameters have been decreased continuously with increased defect density.

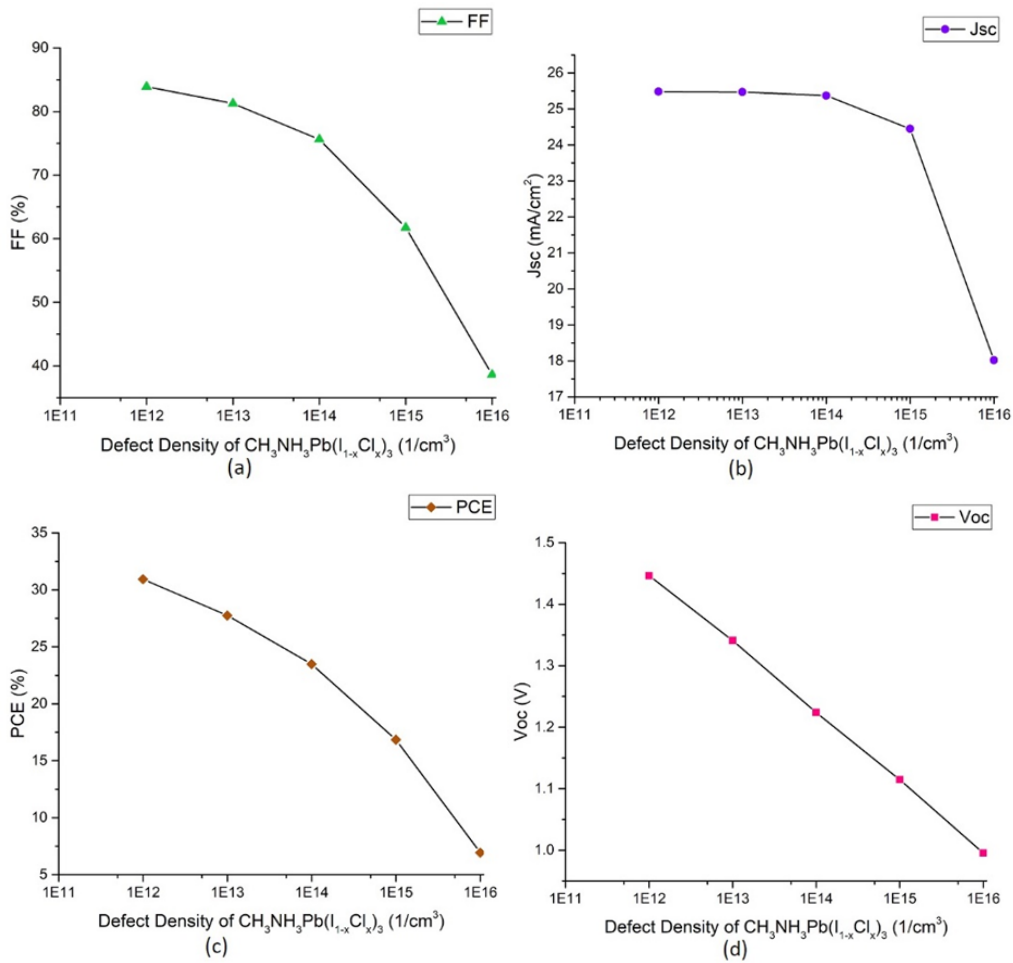


Figure3. Showing the variation of Solar cell parameters with respect to defect density of PAL.(a) FF with respect to PAL defect density. (b) J_{sc} with respect to PAL defect density (c) PCE with respect to PAL defect density.(d) V_{oc} with respect to PAL defect density.

When defect density is $> 1 \times 10^{14} \text{ cm}^{-3}$, J_{sc} is almost constant but further increase in defect density causes drastically reduction in J_{sc} from $25.481 \text{ mA}/\text{cm}^2$ to $18.026 \text{ mA}/\text{cm}^2$. It is seen that V_{oc} has decreased from 1.446 V to 0.995 V and PCE decreased from 30.93% to 6.93% with increasing defect density of PAL from $1 \times 10^{12} \text{ cm}^{-3}$ to $1 \times 10^{16} \text{ cm}^{-3}$. Decrease of 53.96% in FF is obtained by increasing defect density from $1 \times 10^{12} \text{ cm}^{-3}$ to $1 \times 10^{16} \text{ cm}^{-3}$. As seen from the above the performance parameters of PSC depends tremendously on defect density of PAL.

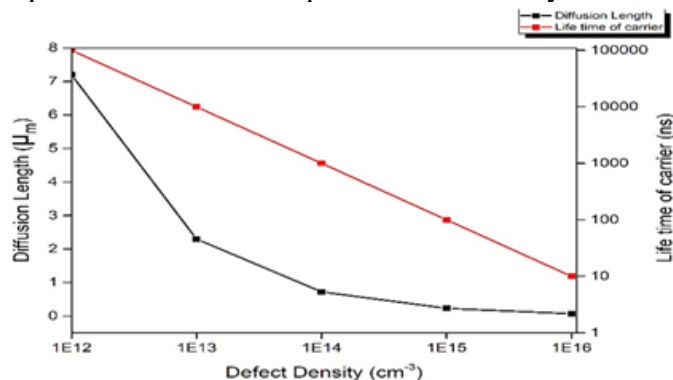


Figure 4. Showing variation in diffusion length and life time of the carrier with variation of defect density of PAL

Here effect on diffusion length and life time of the carrier is investigated by varying the defect density of the PAL. From the fig.4 it is seen that increase in defect density of PAL caused reduced

diffusion length of the carriers. Higher diffusion length indicates longer lifetime of the carrier and here diffusion length is decreased so the life time of the carrier is also decreased. The contour depicts that increasing the defect density of the PAL causes diffusion length of the carriers as well as the life time of the carrier to decrease.

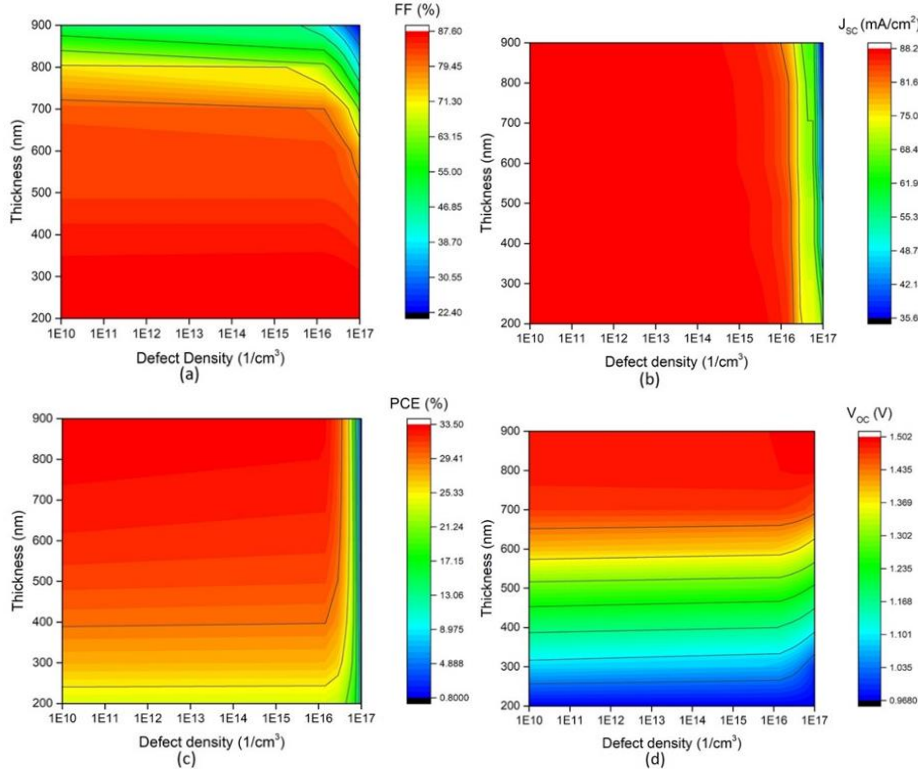


Figure 5. Showing the Contour graph of Solar cell parameters as a joint function of defect density and thickness of PAL.(a) Contour of FF with respect to joint function of defect density and thickness of PAL.(b) Contour of J_{SC} with respect to defect density and thickness of PAL (c) Contour of PCE with respect to PAL defect density.(d) Contour of V_{OC} with respect to defect density and thickness of PAL

It is depicted from the contour that when defect density as well as thickness is varied from 10^{10} cm^{-3} to 10^{17} cm^{-3} and 200 nm to 900 nm respectively, the photovoltaic parameters of perovskite material varies, There is a decrease of 24.38% in PCE when thickness is above 500 nm and defect density is varied from 10^{10} cm^{-3} to 10^{16} cm^{-3} . V_{OC} varies from 1.502 V to 0.9680 V as thickness of the PAL is varied from 900 nm to 200 nm . J_{SC} decreases by 59.63% when defect density is varied from 10^{10} cm^{-3} to 10^{17} cm^{-3} . FF is seen to be decreased when thickness of PAL is varied from 200 nm to 900 nm and defect density varied from 10^{10} cm^{-3} to 10^{17} cm^{-3} .

Effect of variations of layer interface defect density between ETL/PAL and PAL/HTL on PSC parameters

Effect of variation of layer defect density between ETL/PAL and PAL/HTL on the PSC parameters, mainly on the PCE is investigated.

Table 2: - Interface layer defect parameters of ETL/ Perovskite and Perovskite/HTL

Parameters	ETL/ Perovskite	Perovskite/HTL
Type of defect	neutral	neutral
Capture cross section of electron (cm^2)	1×10^{-19}	1×10^{-19}
Capture cross section of hole (cm^2)	1×10^{-19}	1×10^{-19}
Energy distribution	Single	Single
Defect energy level reference	Above Highest Ev	Above Highest Ev

Energy level with respect to the Reference (eV)	0.6	0.6
Total density (cm^{-2})	1×10^8 to 1×10^{18}	1×10^8 to 1×10^{18}

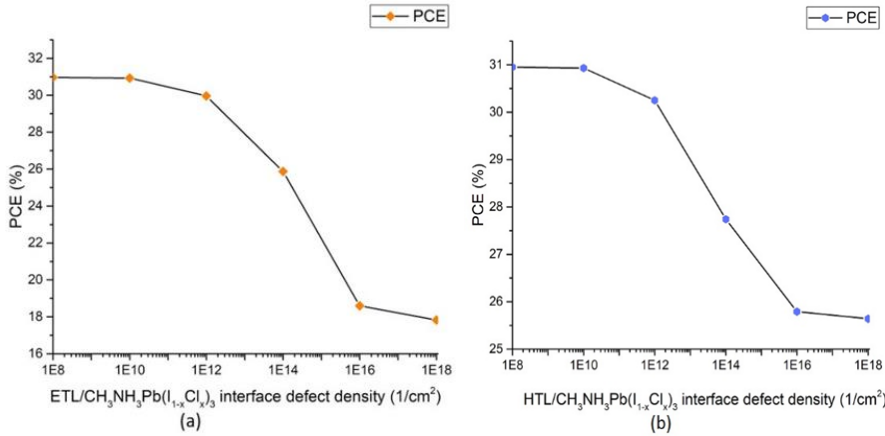


Figure 6. Showing variation in PCE with respect to interface defect density. (a)PCE with respect to interface defect density between ETL/Perovskite. (b) PCE with respect to interface defect density between HTL/Perovskite.

When interface defect density between ETL/ Perovskite is varied from $10^{10} cm^{-2}$ to $10^{16} cm^{-2}$ at the defect energy level of $0.6 eV$, the PCE is decreased continuously, from 30.93% to 18.13% whereas variation of the interface layer defect density between Perovskite/HTL from $10^{10} cm^{-2}$ to $10^{16} cm^{-2}$ caused the PCE to decreased continuously from 30.89% to 25.62%. At the Energy level of $0.6 eV$ with increase of interface defect density of HTL/ Perovskite and ETL/ Perovskite interfaces from $10^{10} cm^{-2}$ to $10^{16} cm^{-2}$ there is a decrease in the PCE of 17.06% and 41.38% respectively. From above result, it is seen that increase in defect density between interfaces of ETL/ Perovskite Caused significant reduction in the PCE in compared to increase in defect density between HTL/ Perovskite layer.

Impact of variations of defect energy level on PSC parameters

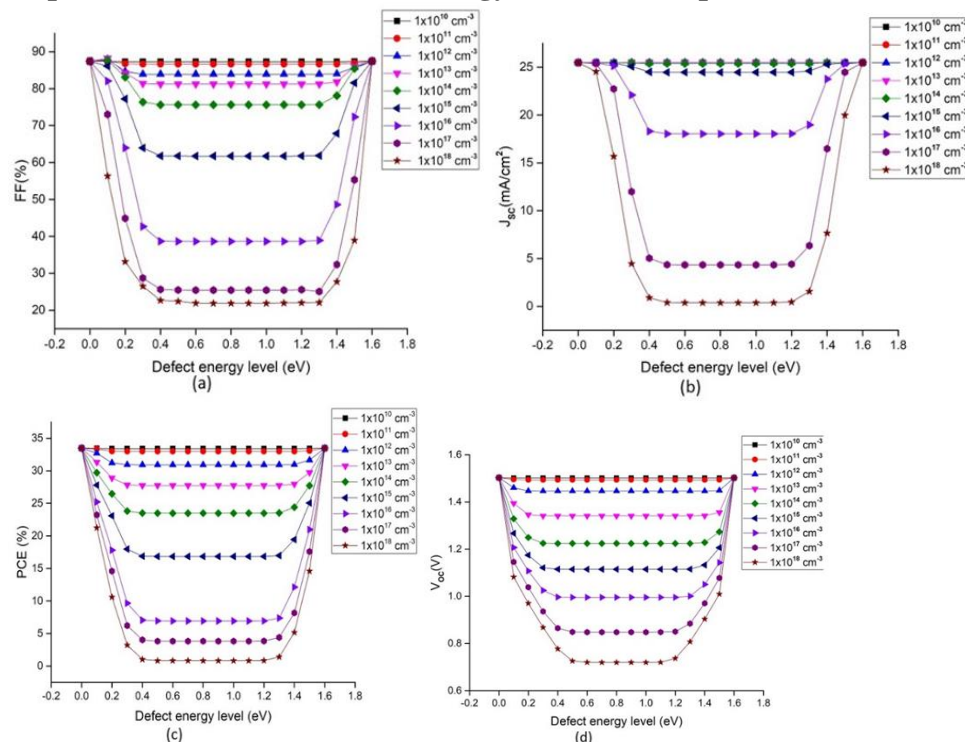


Figure 7. Showing performance of PSC Parameters with various defect energy level and defect density of PAL.(a) FF with respect to different defect energy level and defect density of PAL.(b) J_{SC} with respect to different defect energy level and defect density of PAL (c)Variation of PCE with respect to different defect energy level and defect density of PAL.(d) V_{OC} with respect to different defect energy level and defect density of PAL.

Effect of various Defect energy level with different defect density of PAL has been studied on solar cell parameters i.e V_{OC} , J_{SC} , FF and PCE . From above obtained result it can be concluded that the performance parameters of the perovskite material are not much affected as we increase the defect density of the perovskite from 1×10^{10} to $1 \times 10^{12} \text{ cm}^{-3}$ while increasing the defect energy level of the perovskite material from 0 to 1.8 eV. Further increase in the defect density till $1 \times 10^{15} \text{ cm}^{-3}$ it is obtained that there is change in the parameters of V_{OC} , FF and PCE but J_{SC} is not much affected. There is a decrease of 50.21% in PCE as we increase the defect density from 1×10^{10} to $1 \times 10^{15} \text{ cm}^{-3}$. For defect energy level from 0.4 eV to 1.2 eV which can be treated as deep energy level all Parameters like V_{OC} , J_{SC} , FF and PCE is constant for a specific defect density of PAL.

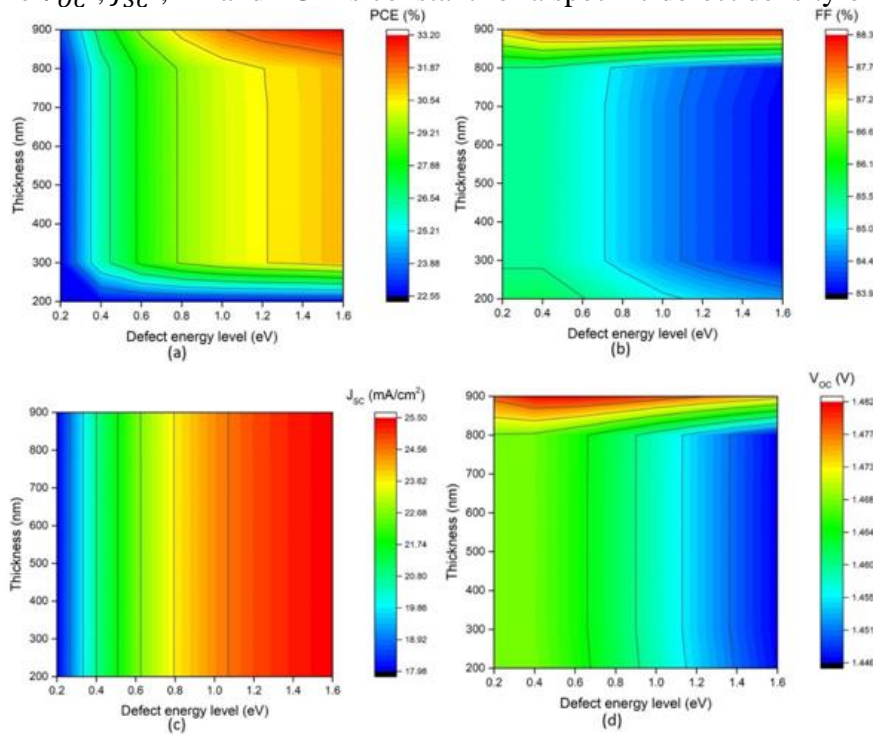


Figure 8. Showing the Contour graph of Solar cell parameters as a joint function of defect energy level and thickness of PAL.(a) Contour of FF with respect to joint function of defect energy level and thickness of PAL.(b) Contour of J_{SC} with respect to defect energy level and thickness of PAL (c) Contour of PCE with respect to defect energy level and thickness of PAL.(d) Contour of V_{OC} with respect to defect energy level and thickness of PAL.

As the defect energy level is varied from 0.4eV to 1.6 eV, there is slight variation in . V_{OC} and FF i.e. V_{OC} varies from 1.482V to 1.446 V and FF varies from 88.3% to 83.9%. PCE varies from 33.2% to 22.5% and J_{SC} varies from 25.5 mA/cm^2 to 17.98 mA/cm^2 .

Table.3. Improvement of PCE over earlier simulated work

Device Structure	V_{oc} (V)	J_{sc} (mA/cm ²)	FF(%)	PCE(%)	References
PEDOT:PSS/Perovskite/CdS	1.2	27	85	25	[15]
FTO/TiO ₂ /PSK/CuI/Au	0.93	18.90	77	16.2	[37]
FTO/ TiO ₂ /MAPbI ₃ /Spiro-OMeTAD/Au)	1.0	20.20	87	18.35	[38]

ITO/ZnO/MAGeI3/Spiro-OMeTAD/Au	1.74	16.27	64.51	18.3	[39]
Glass/FTO/TiO ₂ /CH ₃ NH ₃ Pb(I _{1-x} Cl _x) ₃ /Cu ₂ O/Carbon	1.15	23.34	70.31	18.92	[40]
TiO ₂ /ZnO/MAPbI ₃ / Spiro-OMeTAD/C60	1.1	19.01	88.88	18.52	[41]
FTO/SnO ₂ /(CH ₃ NH ₃ PbI ₃)/CuInSe ₂ /Ag	0.664	45.42	67.42	20.36	[42]
FTO/SnO ₂ /(CH ₃ NH ₃ SnI ₃)/CuInSe ₂ /Ag	0.664	45.5	62.5	18.89	[42]
This Work	1.45	25.48	84	30.93	

Conclusions

An extensive investigation has been done for obtaining a high efficiency device configuration perovskite solar cell and same has been simulated using SCAPS-1D software. The present study using device structure FTO/TiO₂/CH₃NH₃Pb(I_{1-x}Cl_x)₃/Spiro-OMeTAD/Au shows a better solar cell parameter, mainly PCE than earlier works. Different combinations of width and defect density of PAL has been tried to obtain optimized solar cell parameter. The simulation of proposed device structure at the thickness of 900 nm and defect density of $1 \times 10^{12} \text{ cm}^{-3}$ of PAL, provide best possible power conversion efficiency of 30.93%, Voc of 1.45 V and Jsc of 25.48 mA/cm² and FF of 83.92%. This is mainly due to increased charge carrier pairs generation and reduced recombination respectively. It has been found that defect density of PAL is of tremendous effect on improving PCE. The present study will contribute towards the fabrication of highly efficient device of perovskite material CH₃NH₃Pb(I_{1-x}Cl_x)₃, furthermore reduce dependence on fossil fuel and provide insight to researchers to optimize solar cell parameter in future.

References

- [1] S. M. Körbel, M. Marques and S. Botti, J. Mater. Chem. C, “Stability and electronic properties of new inorganic perovskites from high-throughput ab initio calculations”, Journal of Materials Chemistry C, 4, 3157-3167, (2016).
- [2] NG Park, “Perovskite solar cells: an emerging photovoltaic technology,” Materials today, 18 (2), 65-72 (2015).
- [3] P Umari, E Mosconi, F De Angelis, “Relativistic GW calculations on CH₃NH₃PbI₃ and CH₃NH₃SnI₃ Perovskites for Solar Cell Applications,” Scientific Reports, 4, 4467 (2014).
- [4] Faiza Jan Iftikhar, Qamar Wali, Shengyuan Yang, Yaseen Iqbal, Rajan Jose, Shamsa Munir, Irfan A. Gondal, Muhammad Ejaz Khan, “Structural and optoelectronic properties of hybrid halide perovskites for solar cells”, Organic Electronics, 91, 106077 (2021).
- [5] LK Ono, EJ Juarez-Perez, Y Qi, “Progress on perovskite materials and solar cells with mixed cations and halide anions,” ACS Appl. Mater. Interfaces, 9 (36), 30197–30246 (2017).
- [6] TC Sum, N Mathews, “Advancements in perovskite solar cells: photophysics behind the photovoltaics,” Energy Environ. Sci., 7, 2518-2534 (2014).
- [7] A. Kojima, K. Teshima, Y. Shirai, and T. Miyasaka, “Organometal halide perovskites as visible-light sensitizers for photovoltaic cells,” J. Amer. Chem. Soc., 131 (17), 6050–6051 (2009).
- [8] J. Jeng, Y. F. Chiang, M. H. Lee, S. R. Peng, T. F. Guo, P. Chen, and T. C. Wen, “Methylammonium lead iodide perovskite/fullerene-based hybrid solar cells,” SPIE Newsroom, 10 (2), 005033 (2014).
- [9] A. Toshniwal, A. Jariwala, V. Kheraj, A. S. Opanasyuk, and C. J. Panchal, “Numerical simulation of tin based perovskite solar cell: Effects of absorber parameters and hole transport materials,” J. Nano Electron. Phys., 9 (3), 03038 (2017).



- [10] V. D'Innocenzo, G. Grancini, M. J. P. Alcocer, A. R. S. Kandada, S. D. Stranks, M. M. Lee, G. Lanzani, H. J. Snaith, and A. Petrozza, "Excitons versus free charges in organo-lead tri-halide perovskites," *Nature Commun.*, 5, 3586 (2014)
- [11] C. C. Stoumpos, C. D. Malliakas, and M. G. Kanatzidis, "Semiconducting tin and lead iodide perovskites with organic cations: Phase transitions, high mobilities, and near-infrared photoluminescent properties," *Inorganic Chem.*, 52 (15), 9019–9038 (2013).
- [12] H. Oga, A. Saeki, Y. Ogomi, S. Hayase, and S. Seki, "Improved understanding of the electronic and energetic landscapes of perovskite solar cells: High local charge carrier mobility, reduced recombination, and extremely shallow traps," *J. Amer. Chem. Soc.*, 136 (39), 13818–13825 (2014).
- [13] M. Acik and S. B. Darling, "Graphene in perovskite solar cells: Device design, characterization and implementation," *J. Mater. Chem., A*, 4 (17), 6185–6235 (2016).
- [14] A. Kojima, K. Teshima, Y. Shirai, T. Miyasaka, "Organometal halide perovskites as visible-light sensitizers for photovoltaic cells," *J. Am. Chem. Soc.*, 131, 6050–6051 (2009).
- [15] M.S. Chowdhurya,b , S.A. Shahahmadic , P. Chelvanathanb , S.K. Tiong , N. Aminc , K. Techatoa,d,g, N. Nuthammachota, T. Chowdhurye , M. Sukluengf , "Effect of deep-level defect density of the absorber layer and n/i interface in perovskite solar cells by SCAPS 1D," *Results in Physics*, 16, 102839 (2020).
- [16] D. Liu, J. Yang, T.L. Kelly, "Compact layer free perovskite solar cells with 13.5% efficiency," *J. Am. Chem. Soc.*, 136, 17116–17122 (2014).
- [17] D.-H. Kang, N.-G. Park, "On the current–voltage hysteresis in perovskite solar cells: dependence on perovskite composition and methods to remove hysteresis," *Adv. Mater.*, 31, 1805214 (2019).
- [18] F. Zhang, B. Yang, Y. Li, W. Deng, and R. He, "Extra long electron–hole diffusion lengths in $\text{CH}_3\text{NH}_3\text{PbI}_3 \times \text{Cl}_x$ perovskite single crystals," *J. Mater. Chem. C*, 5 (3), 8431–8435 (2017).
- [19] E. M. Hutter, G. E. Eperon, S. D. Stranks, and T. J. Savenije, "Charge carriers in planar and meso-structured organic–inorganic perovskites: Mobilities, lifetimes, and concentrations of trap states," *J. Phys. Chem. Lett.*, 6 (15), 3082–3090 (2015).
- [20] H.-S. Kim, C.-R. Lee, J.-H. Im, K.-B. Lee, T. Moehl, A. Marchioro, S.-J. Moon, R. Humphry-Baker, J.-H. Yum, J. E. Moser, M. Grätzel, and N.-G. Park, "Lead iodide perovskite sensitized all-solid-state submicron thin film mesoscopic solar cell with efficiency exceeding 9%," *Sci. Rep.*, 2 (1), 591 (2012).
- [21] M. M. Lee, J. Teuscher, T. Miyasaka, T. N. Murakami, and H. J. Snaith, "Efficient hybrid solar cells based on meso-superstructured organometal halide perovskites," *Science*, 338 (6107), 643–647 (2012).
- [22] W. S. Yang, B.-W. Park, E. H. Jung, N. J. Jeon, Y. C. Kim, D. U. Lee, S. S. Shin, J. Seo, E. K. Kim, J. H. Noh, and S. I. Seok, "Iodide management in formamidinium-lead-halide-based perovskite layers for efficient solar cells," *Science*, 356 (6345), 1376–1379 (2017).
- [23] H.-S. Duan, H. Zhou, Q. Chen, P. Sun, S. Luo, T.-B. Song, B. Bob, an Y. Yang, "The identification and characterization of defect states in hybrid organic–inorganic perovskite photovoltaics," *Phys. Chem. Chem. Phys.*, 17 (1), 112–116 (2015).
- [24] N. Torabi et al., "Development of a silver/polymer nanocomposite interconnection layer for organic tandem solar cells," *J. Nanophotonics*, 9 (1), 093049 (2015).
- [25] M.M. Tavakoli, P. Yadav, R. Tavakoli, J. Kong, "Surface engineering of TiO_2 ETL for highly efficient and hysteresis-less planar perovskite solar cell (21.4%) with enhanced open-circuit voltage and stability," *Adv. Energy Mater.*, 8 (23), 1800794 (2018).
- [26] J.W. Lee, H.S. Kim, N.G. Park, "Lewis acid-base adduct approach for high efficiency perovskite solar cells," *Acc. Chem. Res.*, 49 (2), 311–319 (2016).



- [27] Y.Y. Zhang, S. Chen, P. Xu, H. Xiang, X.G. Gong, A. Walsh, S.H. Wei, Intrinsic instability of the hybrid halide perovskite semiconductor $\text{CH}_3\text{NH}_3\text{PbI}_3^*$, *Chin. Phys., Lett.* 35 (3), 036104 (2018).
- [28] A. Buin, R. Comin, J. Xu, A.H. Ip, E.H. Sargent, "Halide-dependent electronic structure of organolead perovskite materials," *Chem. Mater.*, 27 (12), 4405–4412 (2015).
- [29] S. Maniarasu, M.K. Rajbhar, R.K. Dileep, E. Ramasamy, G. Veerappan, "Hole conductor free ambient processed mixed halide perovskite solar cells," *Mater. Lett.*, 245, 226–229 (2019).
- [30] P. Docampo, F.C. Hanusch, S.D. Stranks, M. Doblinger, J.M. Feckl, M. Ehrensperger, N.K. Minar, M.B. Johnston, H.J. Snaith, T. Bein, "Solution Deposition-conversion for planar heterojunction mixed halide perovskite solar cells," *Adv. Energy Mater.*, 4 (14), 1400355 (2014).
- [31] Yuan Li, Haoyuan Li, Cheng Zhong, Gjergji Sini & Jean-Luc Brédas, "Characterization of intrinsic hole transport in single-crystal spiro-OMeTAD," *npj Flexible Electronics.* 1, 2 (2017).
- [32] A. Husainat et al., "Simulation and Analysis of Methylammonium Lead Iodide Perovskite Solar Cell with a Contact Using SCAPS 1D Simulator," *Am. J. Opt. Photonics.* 7 (2), 33-40 (2019).
- [33] M. S. S. Basyoni et al., "On the Investigation of Interface Defects of Solar Cells: Lead-Based vs Lead-Free Perovskite," in *IEEE Access.* 9, 130221-130232 (2021).
- [34] Asif Hossain, Muhammad Mahmudul Hasan, MD Shaikh Rahman, M. A. Munaim Hossain, "Fully Lead-Free All Perovskite Tandem Solar Cell with Improved Efficiency: Device Simulation Using SCAPS-1D," 2020 IEEE Region 10 Symposium (TENSYMP). 1221-1224 (2020).
- [35] M Ayad, M Fathi, A Mellit, "Study and performance analysis of Perovskite solar cell - structure based on organic and inorganic thin films," *Optik.* 233, 166619 (2021).
- [36] N. Kour, R. Mehra, and Chandni, "Efficient design of perovskite solar cell using mixed halide and copper oxide," *Chin. Phys. B.* 27 (1), 018801 (2018).
- [37] L. Zhu, G. Shao, and J. Luo, "Numerical study of metal oxide heterojunction solar cells," *Semiconductor Science and Technology,* 26 (8), 085026 (2011).
- [38] MI Hossain, FH Alharbi, N Tabet, "Copper oxide as inorganic hole transport material for lead halide perovskite based solar cells," *Solar Energy.* 120, 370-380 (2015).
- [39] Sagar Bhattarai, T.D. Das, "Optimization of the perovskite solar cell design to achieve a highly improved efficiency," *Optical Materials.* 111, 110661 (2021).
- [40] Shambhavi Rai, B.K. Pandey, D.K. Dwivedi., "Modeling of highly efficient and low cost $\text{CH}_3\text{NH}_3\text{Pb}(\text{I}-\text{xCl}_\text{x})_3$ based perovskite solar cell by numerical simulation," *Optical Materials,* 100, 109631 (2020).
- [41] Sagar Bhattarai, Arvind Sharma, T.D. Das, "Efficiency enhancement of perovskite solar cell by using doubly carrier transport layers with a distinct bandgap of MAPbI_3 active layer," *Optik,* 224, 165430 (2020).
- [42] Gagandeep, Mukhtiyar Singh, Ramesh Kumar, Vinamrita Singh, "Investigation of $\text{CH}_3\text{NH}_3\text{PbI}_3$ and $\text{CH}_3\text{NH}_3\text{SnI}_3$ based perovskite solar cells with CuInSe_2 nanocrystals," *Optik,* 246, 167839 (2021).